JCI The Journal of Clinical Investigation

# Intermittent glucocorticoid treatment improves muscle metabolism via the PGC1α/Lipin1 axis in an aging-related sarcopenia model

Ashok Daniel Prabakaran, … , Brian N. Finck, Mattia Quattrocelli

*J Clin Invest.* 2024. https://doi.org/10.1172/JCI177427.

Research In-Press Preview Aging Muscle biology

## Graphical abstract

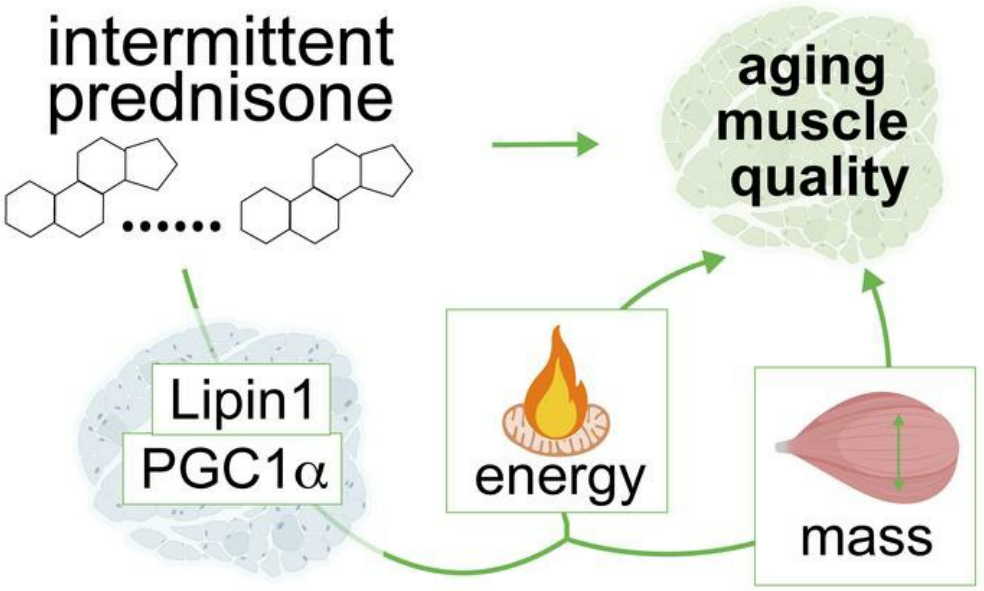

# Intermittent glucocorticoid treatment improves muscle metabolism via the PGC1alpha/Lipin1 axis in an aging-related sarcopenia model

**Authors:** Ashok Daniel Prabakaran[1], Kevin McFarland[1], Karen Miz[1], Hima Bindu Durumutla[1], Kevin Piczer[1], Fadoua El Abdellaoui Soussi[1], Hannah Latimer[1], Cole Werbrich[1], Hyun-Jy Chung[1], N. Scott Blair[1], Douglas P. Millay[1], Andrew J. Morris[2], Brendan Prideaux[3], Brian N. Finck[4], Mattia Quattrocelli[1,*]

**Affiliations:**

[1] Molecular Cardiovascular Biology, Heart Institute, Cincinnati Children's Hospital Medical Center and Dept. Pediatrics, University of Cincinnati College of Medicine, Cincinnati, OH, USA;

[2] Dept. Pharmacology and Toxicology, UAMS College of Medicine and Central Arkansas VA Healthcare System, Little Rock, AR, USA;

[3] Dept. Neuroscience, Cell Biology, and Anatomy, University of Texas Medical Branch (UTMB), Galveston, TX, USA;

[4] Dept. Medicine, Center for Human Nutrition, Washington University in St Louis, MO, USA.

*** Corresponding Author:** Mattia Quattrocelli, PhD, Molecular Cardiovascular Biology, Heart Institute, Cincinnati Children's Hospital Medical Center, 240 Albert Sabin Way T4.676, Cincinnati, OH 45229. Email: mattia.quattrocelli@cchmc.org, tel: +1-513-517-1221.

**Keywords –** Sarcopenia, glucocorticoid steroids, glucocorticoid receptor, muscle mitochondria, muscle mass, sarcopenia, PGC1alpha isoforms, Lipin1.

**Conflicts of interest –** MQ is listed as co-inventor on a patent application related to intermittent glucocorticoid use filed by Northwestern University (PCT/US2019/068618). All other authors declare no competing interests.

**Abstract**

Sarcopenia burdens the elderly population through loss of muscle energy and mass, yet treatments to functionally rescue both parameters are missing. The glucocorticoid prednisone remodels muscle metabolism based on frequency of intake, but its mechanisms in sarcopenia are unknown. We found that once-weekly intermittent prednisone rescued muscle quality in aged 24-month-old mice to levels comparable to young 4-month-old mice. We discovered an age- and sex-independent glucocorticoid receptor transactivation program in muscle encompassing PGC1alpha and its co-factor Lipin1. Treatment coordinately improved mitochondrial abundance through isoform 1 and muscle mass through isoform 4 of the myocyte-specific PGC1alpha, which was required for the treatment-driven increase in carbon shuttling from glucose oxidation to amino acid biogenesis. We also probed the myocyte-specific Lipin1 as non-redundant factor coaxing PGC1alpha upregulation to the stimulation of both oxidative and anabolic effects. Our study unveils an aging-resistant druggable program in myocytes to coordinately rescue energy and mass in sarcopenia.

**Brief summary**

Intermittent prednisone coordinates mitochondrial and mass rescue in sarcopenia by transactivating the PGC1alpha-Lipin1 axis in myocytes.

**Graphical abstract**

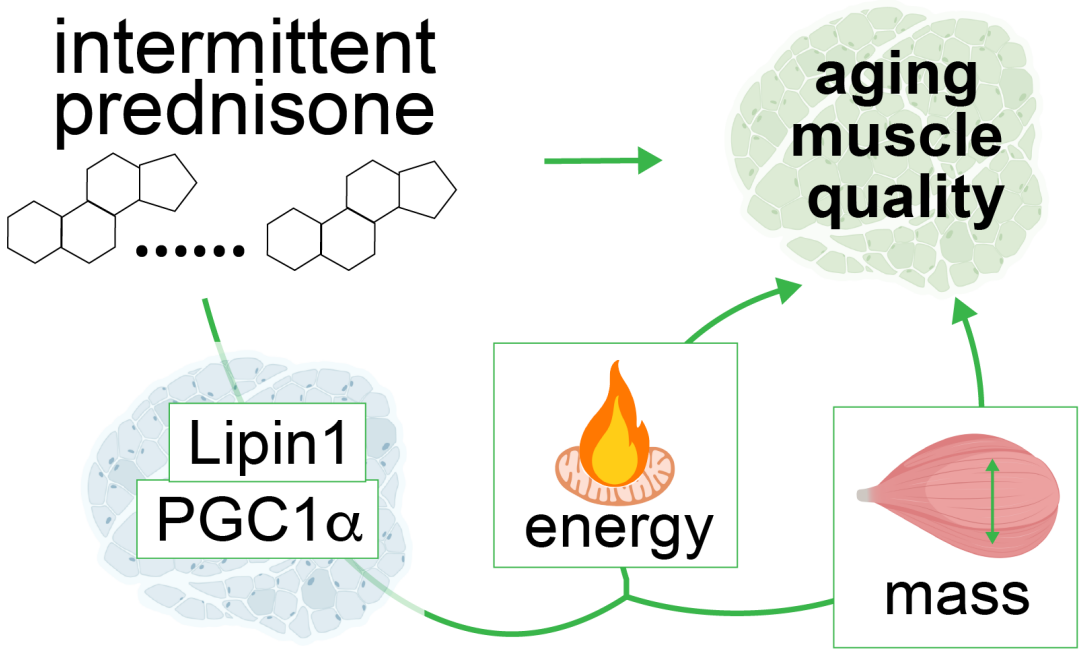

## Introduction

Aging-related sarcopenia contributes to loss of mobility and affects lifestyle in the elderly population (1). With aging, muscle loses both mass and quality, i.e. intrinsic capacity of generating force (2). Indeed, sarcopenia correlates with impaired metabolic capacity to produce energy in muscle (3, 4). However, the reciprocal regulations between metabolic capacity and mass remodeling in muscle aging remain largely unelucidated.

The peroxisome proliferator-activated receptor-gamma coactivator 1 alpha (PGC1alpha) is a major regulator of mitochondrial biology through at least two splice variants (5): the canonical longer PGC1alpha-isoform 1 regulates mitochondrial biogenesis and function, while the shorter PGC1alpha-isoform 4 (6) increases muscle mass and strength in cachectic muscle (7) and sarcopenia (8). While the role of PGC1alpha in mitochondrial capacity (9) and overall mitochondrial protein quality (10) is quite established, its effects on age-related sarcopenia and weakness are still debated with conflicting results. Studies in aging transgenic mice reported gain of muscle mass with constitutive PGC1alpha overexpression (11) and, conversely, loss of lean mass with constitutive muscle PGC1alpha knockout (12). However, another study with constitutive PGC1alpha overexpression versus knockout in muscle showed that PGC1alpha was dispensable for age-related sarcopenia (13). Another recent study showed that lifelong muscle PGC1$\alpha$ overexpression increased muscle mass in males but not females, and improved muscle fatigue at the expense of specific force (14). Thus, the role of myocyte-specific PGC1alpha in rescuing age-related sarcopenia and weakness remains unclear. This opens the question of whether additional factors balance the PGC1alpha action on energy and mass in muscle.

Lipin1 is a multi-functional protein that regulates muscle function and bioenergetics, and its ablation leads to muscle dysfunction and lipid accumulation in mice (15). Lipin1 acts in the cytosol as a phosphatidic acid phosphohydrolase (16, 17) and in the nucleus as a regulator of gene transcription (18). In muscle, Lipin1 regulates many complex processes, including myofiber stability and regeneration (19), as well as autophagy/mitophagy (20, 21). In hepatocytes, Lipin1 co-activates PGC1alpha through a direct protein-protein interaction (18), but this role of Lipin1 remains unexplored in muscle. More generally, the role of the myocyte-specific Lipin1 in muscle aging and energy-mass balance requires further investigation.

Glucocorticoid steroids are potent drugs that regulate both energy metabolism and mass. Dosing frequency of glucocorticoid intake determines the benefits/risks ratio of these drugs with regards to metabolic balance. Chronic once-daily glucocorticoid intake promotes metabolic

imbalance (22). Conversely, dosing intermittence shifts the glucocorticoid metabolic program from pro-wasting, i.e. atrophy and decreased bioenergetics with once-daily prednisone, to pro-ergogenic, i.e. increased bioenergetics and muscle mass with once-weekly prednisone in young adult mice, counteracting the muscle detriments induced by diet-induced obesity (23). In dystrophic patients, a recent pilot clinical trial reported positive trends in both lean mass and mobility with once-weekly prednisone (24). However, relevance and myocyte-autonomous mechanisms of glucocorticoid intermittence in the context of muscle aging are still unknown.

Here we report on the rejuvenating effects of intermittent prednisone on both bioenergetics and mass in the aging muscle of male and female mice. We interrogated transcriptomic and epigenomic datasets to identify activation of Lipin1-PGC1alpha axis. We used inducible myocyte-specific knockout models for PGC1alpha and Lipin1 to investigate requirement of these factors for the coordinated rescue of energy and mass in the absence of developmental or lifelong muscle adaptations to the manipulation of those genes. Moreover, we found that the PGC1alpha upregulation mediates the boost in amino acid biogenesis from oxidative intermediates, linking the bioenergetic and anabolic stimulations of treatment in muscle. Our study provides evidence and myocyte-specific mechanisms to challenge existing paradigms on glucocorticoid drugs with unexpected anti-sarcopenic effects.

## Results

*Intermittent once-weekly prednisone rejuvenates mitochondrial and mass properties of the aging muscle.*

Muscle aging is characterized by declines in both mitochondrial capacity and mass (25). Based on the initial positive effects we documented on both mitochondrial function and mass in young adult muscle of WT mice (26), we tested the extent to which an intermittent once-weekly prednisone treatment impacted muscle properties in the context of aging. We treated aged WT mice at 24 months of age and background-matched (*C57BL/6JN*) young adult controls at 4 months of age, all from the National Institute on Aging's Division of Aging Biology mouse colony. Treatment was consistent with our prior report (26), i.e. once-weekly 1mg/kg prednisone i.p. at ZT0 for 12 weeks, controlled by the same schedule of vehicle administration. Pre/post non-invasive physiological assessments were conducted at 72-24hrs prior the first drug injection and at 24hrs after the last injection, which immediately preceded invasive assessments. We treated males and females in parallel and we report sex-disaggregated data in **Fig. 1** and **Suppl. Fig. 1**.

As parameters of overall strength and function, we quantitated grip strength and treadmill performance at baseline and after treatment (i.e. ~27 months of age in older mice), and quantitated force production in situ in tibialis anterior muscles after treatment. In the absence of treatment (vehicle), compared to young controls, older mice showed decreased strength and treadmill endurance at start and a decline at endpoint. Compared to vehicle, treatment increased both parameters in older mice at endpoint compared to start. The values for treated older mice were not significantly different from the values exhibited by the control vehicle young mice at endpoint. As a validation, the treatment effect was recapitulated in the young mice **(Fig. 1A)**. At endpoint, we used isometric contraction assessments to profile force production through both force-frequency and fatigue assays. Treatment improved specific force in older muscle to levels like the ones shown by the control young muscle, while resistance to fatigue was improved by treatment to similar extents in both age groups **(Fig. 1B).**

We then analyzed mitochondrial properties consistently with our previous treatment study (26). We measured relative trends in mitochondrial abundance through mtDNA/nDNA (mitochondrial/nuclear DNA) qPCR quantitation and unbiased Mitotracker fluorometry in parallel in isolated myofibers from the flexor digitorum brevis muscles. Together with Mitotracker, MitoSOX fluorometry was used to quantitate mitochondrial superoxide production. Treatment increased mitochondrial abundance in both age groups, rescuing the values of treated older muscles to young control-like levels. Conversely, mitochondrial superoxide production was decreased by treatment in older

muscle, suggesting functional coupling in the overall mitochondrial pool after treatment **(Fig. 1C)**. This was further elucidated in quadriceps muscle by respirometry curves with isolated mitochondria (fuel: pyruvate) and NMR-based quantitation of the energy-exchange molecules ATP and phosphocreatine. Treated aging muscle showed young control-like levels of ADP-fueled respiratory control ratio (state III/state$IV_o$, (27)) and static levels of ATP and phosphocreatine **(Fig. 1D)**.

We then analyzed parameters of lean and muscle mass. Using echoMRI, we found that treatment increased overall lean mass in treated older mice to levels like the ones found in young control mice **(Fig. 1E)**. The trends in lean mass were matched by analogous trends in muscle/body weight ratios throughout the body, as shown by measures in four different locomotory muscles (gastrocnemius, quadriceps, triceps, and tibialis anterior) and the respiratory muscle diaphragm **(Fig. 1F)**. The trends in muscle/body weight were further matched by analogous trends in myofiber cross-sectional area, as shown in the case of tibialis anterior **(Fig. 1G)**, further illustrating the treatment-driven rescue of aging muscle mass towards young control-like levels. Discussed so far were treatment effects in male cohorts, but analogous trends were recorded in parallel for age- and background-matched female cohorts from the same colony **(Suppl. Fig. 1)**.

Considering the effects on muscle mass and mitochondrial function, we tested markers of autophagy (LC3B), mitophagy (Pink1), mitochondrial fusion (Mfn2) and fission (Fis1); mitochondrial complex content; independence of muscle mass trends from body weight shifts; relative abundance and cross-sectional area of myofiber types. Treatment increased LC3B-II/-I and Pink1 protein levels in young and aged muscles, while slight changes in Mfn2 and Fis1 were not significant **(Suppl. Fig. 2A)**, suggesting that the increases in muscle and mitochondrial abundance were balanced by a compensatory uptick in autophagy and mitophagy without major changes in the mitochondrial fusion/fission cycle. Cumulative mitochondrial complex signal was increased by treatment in whole lysates and mitochondrial fractions of quadriceps muscle samples **(Suppl. Fig. 2A)**, consistent with the parallel increases of mitochondrial abundance in whole tissue and respiration capacity in fixed mitochondrial amounts. The trends in overall muscle masses appeared independent from body weight shifts as they were recapitulated when muscle weights were normalized to tibia lengths in a subset of mice **(Suppl. Fig. 2B)**. Moreover, we did not record sizable treatment effects on top of the expected age-related shifts in relative myofiber type abundances in two locomotory muscles with mixed fiber typing, i.e. gastrocnemius and triceps, in both sexes **(Suppl. Fig. 3)**. In those muscles, aging decreased CSA in type 2B and 2A myofibers, and treatment increased CSA in type 1, 2A and 2B myofibers **(Suppl. Fig. 3)**, consistently with previously reported effects of sarcopenia and exercise-mediated rescue on murine aging myofiber types (28).

Thus, according to the drug schedule and readout parameters tested here, intermittent prednisone "rejuvenated" both mitochondrial function and mass in the aging muscle, i.e. improved parameters in treated older muscles to young control-like levels.

*Treatment induces a muscle GR program increasing PGC1alpha-Lipin1 expression through aging.*

To gain insight in the mechanisms mediating the dual treatment effects on energy and mass in aging muscle, we profiled the epigenomic signal of the glucocorticoid receptor (GR) in all age/sex/treatment cohorts, in parallel with bulk transcriptomic profiling through RNA-seq in quadriceps muscles from the same mice. Samples were collected at 4-hours after last drug/vehicle injection. Unbiased motif analysis showed the GR-binding element (GRE) motif as the top enriched motif in all groups **(Fig. 2A)** and peak tracks showed clear strong GR peaks upstream of the canonical GR marker *Fkbp5* **(Fig. 2B)**, indicating reliable GR ChIP-seq datasets for further quantitative comparisons.

We first asked whether aging changed the muscle GR epigenomic activity in terms of peak number, signal on GREs and locus distribution at baseline and after treatment. Treatment increased GR peak number and average GR signal enrichment on the GRE motif genome-wide compared to vehicle in both young and aging muscle, but we did not find an age-specific effect in either vehicle- or treated-muscles **(Fig. 2C-D)**. Similarly, compared to vehicle, treatment increased GR signal in promoter-5'UTR rather than intergenic regions, but once again we did not find an age-specific effect in this shift **(Fig. 2E)**. Also, the trends were comparable in both male and female muscles **(Fig. 2C-E)**.

We then sought to overlay the GR ChIP-seq datasets with RNA-seq datasets to identify which GR targets were changing expression levels by treatment in both age groups in both sexes. Principal component analysis of the RNA-seq datasets showed overall sample clustering according to age, treatment, and sex **(Fig. 2F)**. We overlayed GR ChIP-seq and RNA-seq following this question: how many/which genes are changed by treatment across age/sex groups with regards to differential RNA expression and increased GR signal in their promoter-5'UTR region?

We found that approximately 40% of the differentially expressed (DE) genes across all age/sex groups had increased GR signal in their promoter-5'UTR region. When compiling these gene lists together and analyzing them for pathway enrichment through gene ontology (GO), we found several pathways enriched related to muscle regulation and metabolism **(Fig. 2G)**. Considering the potential relevance of these pathways to the treatment-induced phenotype across aging, we used these GO pathways, i.e. the genes found enriched by GO analysis in these pathways, to filter out

potential hits in play here. We confirmed several targets that we reported transactivated by intermittent prednisone in previous reports, including *Anxa1/6* (29), *Klf15* (30), *Nampt* (26) and *AdipoR1* (23) **(Suppl. Fig. 4A)**.

However, we focused on the emergence of *Ppargc1a* (encoding PGC1alpha) and *Lpin1* (encoding Lipin1) among the top hits **(Fig. 2H)** based on two additional findings and literature-informed considerations. On one hand, running the isoform specific analyses from our paired-end RNA-seq datasets, we found that both the canonical mitochondria-regulating isoform 1 and the mass-regulating isoform 4 (7) were increased by treatment in both age groups and, consistent with the idea of double isoform transactivation, treatment increased GR peaks on both proximal (isoform 1) and distal (isoform 4) *Ppargc1a* TSS regions (6) in both young and aging muscle **(Fig. 2I; Suppl. Fig. 4B)**. On the other hand, Lipin1 is a PGC1alpha co-factor and potentiates PGC1alpha activity through direct protein-protein interaction (18). We found that treatment increased GR transactivation of *Lpin1* in both ages, rescued the aging effect on *Lpin1* expression decrease in muscle **(Suppl. Fig. 5A)** and rescued the levels of PGC1alpha binding to Lipin1 **(Suppl. Fig. 5B)**. Moreover, in each of the sequences underlying the identified GR peaks, we found a canonical GRE (ACAnnnTGT). Through luciferase assays with control and GRE-deleted constructs, we found that all three ChIP-seq identified GR-bound GREs were responsive to prednisone in vitro in C2C12 myoblasts through the GRE sequence **(Suppl. Fig. 5C)**. Furthermore, the oxidative boost dependent on the Lipin1-PGC1alpha interaction correlates with triacylglycerol decrease (18). We confirmed this in a subset of control vs treated quadriceps muscles in the aged male cohort through untargeted lipidomics, which revealed a remarkable decrease across 47 triacylglycerol species in treated aged muscles **(Suppl. Fig. 6A)**.

Thus, epigenomic and transcriptomic profiling identified a GR program that is elicited by intermittent prednisone and regulates muscle function and metabolism across aging. Intriguingly, we found a marked GR transactivation of PGC1alpha-Lipin1 and, in the next experiments, we sought to determine their role in the aging muscle rescue enabled by treatment.

*Muscle PGC1alpha is required by intermittent prednisone to coordinately stimulate energy and mass in muscle*

To probe the extent to which PGC1alpha mediates the effects of chronic intermittent prednisone in muscle, we derived mice with myocyte-specific inducible deletion of PGC1alpha by crossing *Ppargc1a*$^{fl/fl}$ (31) with *ACTA1-MerCreMer*$^{+}$ mice (32) on the C57BL/6J background. This background is slightly different than the one of the WT mice used in the young/aged cohorts, but i) it is consistent with all our other transgenic lines, including the Lipin1-KO used also in this study,

and ii) the non-ablated control mice on this background recapitulated all the treatment features that we described above for mice on the 6JN background (see below). PGC1alpha ablation was induced starting at 3 months of age using intra-peritoneal (20 mg/kg per day for 5 days) and then chow-mediated intake (40mg/kg) of tamoxifen for 14 days, followed by 14 days of washout. These conditions allow us to reduce PGC1alpha levels in whole quadriceps muscle lysates by ~85%, as we reported before (26). In this study, we compared *Cre*$^{+/-}$*;Ppargc1a*$^{wt/wt}$ (PGC1alpha-WT) vs *Cre*$^{+/-}$*;Pparcg1a*$^{fl/fl}$ (PGC1alpha-KO) male littermates after tamoxifen/washout to take into account both tamoxifen and Cre presence in both cohorts. After ablation/washout, mice were then started on 12-week-long regimens of intermittent prednisone/vehicle from 4 months of age, the same age/treatment conditions used in the young cohorts of the previous experiment. We used this timeline to minimize the adult muscle adaptations to gene ablation before treatment effects. Considering the epigenomic/transcriptomic screening of the initial cohorts considered targets common to both sexes, in these subsequent mechanistic experiments we focused on only one sex (males) to maintain power to detect trends while decreasing the overall number of mice.

The *Pparcg1a*-floxed allele features *loxP* sites surrounding exons 3-5, which are shared by the transcripts of both isoforms 1 and 4 (7). We therefore verified that both transcripts were deleted in our PGC1alpha-KO muscles at baseline. Compared to PGC1alpha-WT, PGC1alpha-KO muscle showed profound downregulation of total *Ppargc1a*, as well as isoform1 and isoform4 transcripts **(Fig. 3A)**, as assessed through qPCR using previously reported discriminating primers (7). Regarding overall function, despite no differences induced by genotype at baseline and endpoint (i.e. WT vehicle vs KO vehicle), PGC1alpha ablation blocked the treatment effect in both grip strength and treadmill tests **(Fig. 3B)**. Regarding force production, PGC1alpha ablation did not change specific force while did decrease fatigue resistance in vehicle-treated mice, and further blocked the treatment effect on increases in both parameters **(Fig. 3C)**.

Previously, we found that myocyte PGC1alpha is required for the mitochondrial effects of a single circadian-specific glucocorticoid pulse (26). We therefore checked whether this was still true for the chronic intermittent prednisone treatment effects on muscle mitochondria. Indeed, consistent with the finding of PGC1alpha transactivation by chronic treatment, PGC1alpha ablation blocked the treatment effect on mitochondrial abundance, respiratory control ratio of isolated mitochondria and basal oxygen consumption of quadriceps muscle tissue **(Fig. 3D)**. The KO effects on respiration appeared related to overall mitochondrial function rather than shifts in nutrient preference, as they were recapitulated with either glucose/pyruvate or palmitate/palmitoylcarnitine as fuels **(Fig. 3D;** respirometry curves in **Suppl. Fig. 6B)**.

Strikingly, PGC1alpha ablation also blocked the treatment effects on lean and muscle mass.

Despite no genotype differences in vehicle-treated mice, PGC1alpha ablation blocked the treatment effect on lean mass, muscle/body weight ratio (shown here for both muscles used for analyses in this model) and myofiber cross-sectional area **(Fig. 3E)**. Moreover, the treatment/KO effects appeared related to anabolic propensity as shown by two independent puromycin-based assays of protein synthesis: protein puromycinylation in quadriceps muscle lysates after in vivo puromycin injection, and ex vivo O-propargyl-puromycin incorporation/fluorometry (33) in live myofibers **(Fig. 3F)**. We did not quantitate significant effects of muscle PGC1alpha ablation at start or endpoint, nor of treatment on fat mass, body weight and food/water intake **(Suppl. Fig. 6C)**.

Thus, inducible PGC1alpha ablation in adult myocytes without long-term and/or developmental adaptations blocks the effects of chronic intermittent prednisone not only on mitochondrial capacity, but also muscle mass.

*PGC1alpha mediates the treatment effect on increased carbon shuttling between oxidative intermediates and amino acids in muscle.*

We were intrigued by the fact that the myocyte-specific PGC1alpha mediated both mitochondrial and mass effects of treatment. We therefore hypothesized that the upregulated PGC1alpha mediated a myocyte-autonomous metabolic program coordinating the increased mitochondrial metabolism with anabolic growth. Amino acid availability determines mass rescue in sarcopenia (34). Intermediary metabolites like pyruvate and TCA cycle intermediates are direct precursors of amino acids like alanine, glutamine, and aspartate, generally decreased in aging muscle (35). We therefore asked whether PGC1alpha coordinated the carbon shuttling from glucose to amino acid biogenesis in treated muscle. To investigate this in our transgenic muscles, we traced the glucose contribution to in-muscle amino acids using an ex vivo system where the isolated muscle undergoes repetitive contractions in the presence of $^{13}$C-labeled glucose and insulin (30). Albeit not in steady-state, this system offers the advantage of quantitating muscle-autonomous effects without circulating and extra-muscle contributions, and we previously used it to trace macronutrient fate, including glucose, after intermittent prednisone treatments in dystrophic muscles (30) and normal versus obese WT muscles (23).

We compared PGC1alpha-WT/-KO muscles after vehicle/prednisone treatment for labeling rates of glucose intermediates (pyruvate, alpha-ketoglutarate, oxaloacetate) and their putative amino acid products (alanine, glutamate/glutamine, aspartate) downstream of uniformly labeled $^{13}C_6$-glucose. We also quantitated labeling rates for amino acids produced from glycolytic intermediates (serine, glycine). For each metabolite, we quantitated overall fractional labeling i.e. percentage of the sum of all $^{13}$C-labeled isoforms versus the total sum of labeled and unlabeled

isoforms. Compared to vehicle controls, treated PGC1alpha-WT muscles showed increased labeling of the glucose intermediates and their amino acid products, but the treatment effect was blocked or blunted with myocyte PGC1alpha ablation **(Fig. 4A)**. In accordance with the effects of muscle PGC1alpha overexpression/knockout on lactate dehydrogenase isoforms (36), in PGC1alpha-WT muscle treatment (PGC1alpha upregulation) decreased labeling and levels of lactate, while both parameters were increased over WT control levels in both treated and untreated PGC1alpha-KO muscle **(Suppl. Fig. 6D)**. No significant treatment or genotype effects were quantitated for labeled serine and glycine **(Fig. 4A)**, and PGC1alpha ablation did not significantly impact the treatment-driven increase in overall glucose tolerance **(Suppl. Fig. 6E)**, supporting the notion of a specific pathway rather than a boost in overall glucose use.

In light of a prior report implicating PGC1alpha in the transcriptional control of the mitochondrial alanine transaminase(37) (gene name, *Gpt2*), we asked whether we could quantitate a PGC1alpha-dependent effect on the mitochondrial enzymes or mitochondrial enzyme isoforms mediating the carbon shuttling between the metabolites and amino acids found enriched in labeling. Therefore, in addition to *Gpt2* (pyruvate <-> alanine), we quantitated expression levels of *Glud1* (alpha-ketoglutarate <-> glutamate), *Glul* (glutamate -> glutamine), *Got2* (oxaloacetate -> aspartate) in the gastrocnemius muscles of the same animals whose quadriceps muscles were used for the glucose tracing experiments. For all those four enzymes, PGC1alpha ablation blocked or blunted the treatment-driven upregulation seen in PGC1alpha-WT muscle **(Fig. 4B, left; Suppl. Fig. 6F)**. Accordingly, we checked against our RNA-seq datasets in young/older mice and found that the same four enzyme genes were upregulated by treatment in muscles of both young and older age groups **(Fig. 4B, right)**. We tested whether the treatment effect on glucose-derived amino acid biogenesis was quantifiable in young and aged muscle. At 24 hours after last treatment injection, we challenged young and aged mice with 1g/kg glucose coupled with 0.5U/kg insulin to maximize muscle glucose uptake across ages and treatment groups. Mass-spec imaging on cryosections from quadriceps muscles collected at 2-hours post-challenge showed increased levels of alanine, glutamate, glutamine, and aspartate after treatment in both young and aged muscles **(Fig. 4C)**.

Thus, the myocyte-specific PGC1alpha mediates the metabolic program enabled by intermittent prednisone in muscle to coordinate mitochondrial metabolism with amino acid biogenesis.

*Myocyte-specific Lipin1 is required for the pro-ergogenic effects of treatment upstream of PGC1alpha*

Considering the combined upregulation of *Ppargc1a* isoforms 1 and 4 by treatment, we asked whether each isoform was sufficient to rescue a specific parameter of treatment effect, i.e.

mitochondrial abundance by isoform 1 and muscle mass by isoform 4. We generated AAVs to overexpress either GFP (control), or *Ppargc1a* isoform 1, or isoform 4 downstream of a *CMV* promoter. Adult myocyte tropism was promoted by using the MyoAAV serotype (38) and confirmed via qPCR in WT muscle tissue at 2 weeks after a single r.o. injection of $10^{12}$vg/mouse (**Fig. 5A, left)**. We then used PGC1alpha-KO mice for a genetic rescue experiment with AAV-overexpression of isoform 1, isoform 4 or both, in vehicle versus treatment conditions. On one hand, isoform 1 was sufficient to enable the treatment effect on mitochondrial abundance but not mass, consistent with the impact of this isoform on oxidative efficiency (39). On the other hand, isoform 4 was sufficient to enable the treatment effect on muscle mass but not mitochondrial abundance, consistent with prior reports (7). Importantly, treatment showed a significant additive effect over the genetic rescue effect **(Fig. 5A, right)**. Through cryo-histology in tibialis anterior and hydroxyproline dosing in gastrocnemius muscles, we did not detect any sizable changes in muscle architecture and fibrosis of the AAV-transduced cohorts **(Suppl. Fig. 7A)**. In addition to our inducible KO data, this rescue experiment confirmed the specific roles of PGC1alpha isoforms 1 and 4 in the combined energy-mass effect of intermittent prednisone. However, the additive effect of treatment over AAV re-expression made us hypothesize that an additional factor induced by treatment is required for fully coaxing the PGC1alpha upregulation to the global anti-sarcopenic effect.

Within that hypothesis, we were intrigued by the emergence of Lipin1 as GR transactivation target with intermittent prednisone in tandem with PGC1alpha in aging muscle. Indeed, prior experiments in liver showed that Lipin1 is a direct co-activator of PGC1alpha through protein-protein interaction and primes it to enhance its pro-metabolic gene program (18). Constitutive knockout of Lipin1 impairs muscle function and mitochondrial metabolism in young and mature adult ages (15). In the context of intermittent prednisone effects, we reasoned that, if PGC1alpha mediates energy-mass coordination and Lipin1 is a critical PGC1alpha co-activator, Lipin1 could also be required for treatment effects.

We generated transgenic mice for myocyte-restricted inducible ablation of Lipin1 by crossing *Lpin1*$^{fl/fl}$ (floxed exon7, complete protein loss (15)) with *ACTA1-MerCreMer*$^{+}$ mice (32) on the C57BL/6J background. We used the same tamoxifen/washout protocol as PGC1alpha-KO and found ~85% Lipin1 ablation in quadriceps muscle **(Suppl. Fig. 7B)**. Consistent with the PGC1alpha-KO experiments, we compared *Cre*$^{+/-}$*;Lpin1*$^{wt/wt}$ (Lipin1-WT) vs *Cre*$^{+/-}$*;Lpin1*$^{fl/fl}$ (Lipin1-KO) male littermates for the effects of a 12-week-long regimen of intermittent prednisone/vehicle from 4 months of age.

Considering the potential involvement of Lipin1 in muscle oxidative capacity, we interrogated the extent to which the myocyte-specific Lipin1 regulated body-wide $VO_2$ at rest and during

aerobic exercise in metabolic cages and treadmill. Indeed, aging-related exercise intolerance is evident in mice through decreases in baseline and maximal $VO_2$ values (40). At rest, intermittent prednisone increased $VO_2$ independent from body mass, while inducible Lipin1 ablation induced a downward trend in the vehicle-treated muscles and further blocked the treatment effect **(Fig. 5B)**. We then tested untrained mice through an acute exercise with stepwise speed ramp-up on a metabolic treadmill. Treatment significantly increased the maximal values of speed, $VO_2$ and work before exhaustion in Lipin1-WT but not Lipin1-KO mice, suggesting a treatment-driven increase in aerobic fitness dependent on the muscle Lipin1 **(Fig. 5C)**.

In parallel to $VO_2$ and exercise capacity trends, Lipin1 ablation blocked the treatment effect on specific force and fatigue, decreasing the resistance to fatigue also in vehicle-treated muscle **(Fig. 5D)**. Also, Lipin1 deletion blocked the treatment effect on ATP and phosphocreatine levels **(Suppl. Fig. 7C)**, as well as on mitochondrial respiratory control ratio **(Fig. 5E)**. Consistently with the KO effect on decreased mitochondrial respiration compared to WT with pyruvate and palmitoylcarnitine, we found increased *Pdk4* and decreased *Cpt1b* expression in Lipin1-KO vs -WT muscles **(Suppl. Fig. 7D)**. Intriguingly and in line with our PGC1alpha findings and Lipin1-PGC1alpha protein-protein interaction findings, Lipin1 ablation also blocked the treatment effect on the muscle mass parameters of muscle/body weight ratios and myofiber cross-sectional area in two different locomotory muscles (tibialis, hind limbs; triceps, fore limbs; **Fig. 5F-G**) without sizable shifts in myofiber typing **(Suppl. Fig. 7E)**. These effects were obtained even though Lipin1 ablation did not significantly change the treatment effect on muscle PGC1alpha isoforms upregulation compared to vehicle control **(Suppl. Fig. 7F)**.

To circle back to our MyoAAV-based experiment with PGC1alpha isoforms, we used Lipin1-KO mice to test the hypothesis that indeed Lipin1 is the non-redundant additional factor underlying the additive treatment effect over PGC1alpha isoform upregulation. We repeated the combined isoform 1+4 overexpression with and without treatment in Lipin1-KO vs -WT mice, using the same timeline and conditions as in the prior experiment in PGC1alpha-KO mice. We monitored mtDNA/nDNA and muscle weight/body weight as indicators of mitochondrial abundance and muscle mass, and grip strength/body weight as indicator of muscle strength. In the presence of MyoAAV-driven upregulation of the PGC1alpha isoforms, treatment induced an additive effect in all those three parameters compared to vehicle only in Lipin1-WT but not Lipin1-KO mice **(Fig. 5H)**, supporting the non-redundant role of Lipin1 in the treatment effect.

Thus, Lipin1 is a GR transactivation target in aging muscle by intermittent prednisone and its inducible post-natal ablation recapitulates the PGC1alpha-mediated role on energy-mass coordination, underscoring Lipin1 as key factor in the treatment-PGC1alpha muscle program.

## Discussion

In aggregate, our data show that exogenous glucocorticoid intermittence can rescue both mitochondrial and mass defects in the aging muscle through the PGC1alpha-Lipin1 axis. Based on the functional improvements recapitulated by treatment to a variable extent in aging mice of both sexes, we focused here on “inclusive” gene programs underlying comparable remodeling across ages and sexes. However, because sex-specific differences can be identified in specific molecular markers of intermittent prednisone effects in young adult mice (41), future studies are warranted to better investigate how aging affects the “exclusive”, sex-dimorphic programs enabled by glucocorticoid intake.

Our findings linking the pro-ergogenic GR program to simultaneous upregulation of both “mitochondrial” and “mass” *Pparcg1a* isoforms argues in favor of two additional concepts to the puzzling role of PGC1alpha in muscle aging. On one hand, our data demonstrate that a balanced upregulation of both isoforms promotes the balanced rescue of both mitochondrial capacity and muscle mass in the context of sarcopenia. On the other hand, the GR engagement on both isoform TSSs by the glucocorticoid regimen we used here (once-weekly 1mg/kg prednisone at ZT0) implicates the myocyte GR as context-specific “additional factor” that coaxes the PGC1alpha isoform regulation with muscle remodeling outputs. Regarding both aspects, our data here pave the way to several compelling questions for the aging muscle, including shared/differential mechanisms of PGC1alpha isoforms and which co-factors are engaged by the GR in beneficial versus deleterious muscle contexts. Our findings are consistent with genetic experiments with PGC1alpha isoforms (6-8, 39). The role of PGC1alpha in mitochondrial proteostasis has emerged as an important determinant of muscle health and exercise efficacy (10). Future studies are warranted to pinpoint the effects of prednisone intermittence on proteostasis in sarcopenia (42).

Furthermore, our study identifies an additional non-redundant factor required for coaxing PGC1alpha activation towards energy-mass rescue in sarcopenia, i.e. Lipin1. Our data implicate *Lpin1* as GR transactivation target in muscle and required non-redundant factor to link PGC1alpha to the pro-ergogenic program enabled by glucocorticoid intermittence in the aging muscle. Considering the recent findings with Lipin1 ablation and complex lipid metabolism in heart (43), future studies are warranted in better identifying how Lipin1 regulates lipotoxicity in sarcopenia.

Glucose metabolism contributes to cell mass during development (44) and – as highlighted by our data – also in aging. The role of the mitochondrial TCA cycle in providing the “building blocks’ for many anabolic pathways is well known (45), yet its role in aging muscle still needs further elucidation. An important question to address in the future will be how glucocorticoid intermittence

regulates the relationship between non-essential and essential amino acids availabilities, an important point for mass regulation and exercise tolerance in the aging muscle (46).

*Limitations of the study* – Our study presents important limitations to keep in mind when interpreting our findings, especially when projecting their translational potential. We used here aging WT mice between 24 and 27 months of age as main model of sarcopenia. While recapitulating several key hallmarks of aging (47), aging mice do not fully mimic the extraordinarily complex biology of human aging. Our omics analyses were limited by the small sample number of three per group. However, we note that the overlay between transcriptomic and epigenomic datasets empowered our datasets to identify genetically actionable myocyte-autonomous targets thanks to the convergence-based analysis, i.e. filtering for convergent treatment trends in young and old, male and female mice. We recognize that three samples per group is insufficient to identify sex-specific differences, which indeed we did not address here. We also acknowledge that our isolated muscle force analyses did not focus on calcium handling, which remains an important parameter to directly address in future studies with glucocorticoids in muscle aging. Also, an important consideration for our mechanistic studies with PGC1alpha and Lipin1 is that our experiments with myocyte-specific inducible ablation were conducted at 4 months of age (young adulthood). This is because our most promising functional treatment phenotypes and epigenomic-transcriptomic screening hits in the aging cohorts were recapitulated in the young adult cohorts too. However, we recognize that this is most likely an oversimplification and that age-matched ablation studies, i.e. ablation at 24 months of age, will shed light over additional molecular mechanisms in play here.

In summary, our study reports on the thought-provoking phenotypes and muscle-autonomous mechanisms of anti-sarcopenic action by exogenous glucocorticoid intermittence. Our findings challenge the current paradigm on glucocorticoids and muscle regulation, opening new myocyte-autonomous perspectives to counteract aging-related exercise intolerance and strength loss.

## Methods

*Sex as biological variable*

We performed the bulk of our background-matched aged vs young mice experiments in both males and females, analyzing and reporting the physiological, molecular and histological assessments as sex-disaggregated. We performed our unbiased omics-based screen unveiling PGC1alpha-Lipin1 as targets based on RNA and epigenetics trends that were applicable to both sexes. Therefore, we used only males in subsequent KO-based proofs of requirement to minimize variability and overall mouse number used.

*Animal handling and treatments*

Consistent with the ethical approvals, all efforts were made to minimize suffering. Euthanasia was performed through carbon dioxide inhalation followed by cervical dislocation and heart removal. Mice were maintained on a 14h/10h light/dark cycle, approximately 22°C constant temperature, and ad libitum access to chow and water. Aged (24 months-old at treatment start) and young control (4 months-old at treatment start) male and female cohorts were obtained from the NIA Aged Rodent Colony, C57BL/6JN background. Mice for mechanistic studies were obtained and interbred from Jackson Laboratories (Bar Harbor, ME) and/or colleagues. PGC1alpha-KO mice and -WT littermates from crossing #025750 and #009666 lines, $Cre^-$ and $Cre^+$ littermates obtained from *Ppargc1a*$^{fl/wt}$ *x Ppargc1a*$^{wt/fl}$*;HSA-MerCreMer*$^{+/-}$ matings. Analogously, we obtained Lipin1-KO mice and -WT littermates from crossing *Lpin1*$^{fl/fl}$ (floxed exon7, complete protein loss (15)) with the HSA-MCM line. Both PGC1alpha- and Lipin1-KO mice were on the C57BL/6J background. Gene ablation was induced starting at 3 months of age using intra-peritoneal (20 mg/kg per day for 5 days; Sigma #T5648) and then chow-mediated intake (40 mg/kg; Harlan #TD.130860) of tamoxifen for 14 days, followed by 14 days of washout (26). Weekly prednisone treatment consisted of once-weekly i.p. injection of 1mg/kg prednisone (#P6254; Sigma-Aldrich; St. Louis, MO) (30). The injectable solution was diluted from a 5mg/ml stock in DMSO (#D2650; Sigma-Aldrich; St. Louis, MO) in 50 ml volume. Injections were conducted at the beginning of the light-phase (ZT0; lights-on). Pre/post non-invasive physiological assessments were conducted at 72-24hrs before the first drug injection and at 24hrs after the last injection. For epigenetic analyses, mice were sacrificed, and tissues harvested at 4-hours (ZT4) after last prednisone injection in chronic or single-pulse treatments. For non-epigenetic-involving experiments, tissues were harvested 24 hours after last prednisone injection in chronic or single-pulse treatments, i.e., ZT0. All in vivo, ex vivo and post-mortem analyses were conducted blinded to treatment groups.

*Analyses of muscle function, lean and muscle mass, myofiber typing*

Our routine procedures concerning body composition, muscle function, mass and myofiber typing can be found as point-by-point protocols here (48). All analyses were conducted blinded to treatment.

*Respirometry with isolated mitochondria and muscle tissue*

Basal tissue OCR values were obtained from basal rates of oxygen consumption of muscle biopsies at the Seahorse XF HS Mini Extracellular Flux Analyzer platform (Agilent, Santa Clara, CA) using previously detailed conditions (30). Nutrients: 5 mM glucose, 1 mM palmitate-BSA (#G7021, #P0500; Millipore-Sigma, St Louis, MO); inhibitors: 0.5 mM rotenone $^{+}$ 0.5 mM antimycin A (Agilent). Respiratory control ratio (RCR) values were obtained from isolated mitochondria from quadriceps muscle tissues through published procedures (27). 2.5 µg mitochondria were used per well, with 20 µL of 50 mM ADP (Sigma #01905), 50 µM Oligomycin (Milipore #495455-10MG), 100 µM Carbonyl cyanide-p-trifluoromethoxyphenylhydrazone (TCI #C3463), and 5 µM Rotenone (Milipore #557368-1GM)/Antimycin A (Sigma #A674-50MG) to yield final concentrations of 5000, 50, 10, and 0.5 µM. Nutrients: 0.5mM pyruvate, 0.1 mM palmitoylcarnitine (#P2256, #61251; Millipore-Sigma, St Louis, MO). Seahorse measurements were conducted blinded to treatment groups.

*Mitochondrial density, NMR, and mass-spec profiling*

The mtDNA/nDNA assay was performed on genomic DNA isolated using the Gbiosciences Omniprep kit (Gbiosciences #786-136), using the primers reported in (49). For the Mitotracker assay, Mitotracker Green FM powder (Invitrogen #M7514) is resuspended in 373 µL of DMSO (Fisher #BP231-100) to obtain a 200 µM concentration. One microliter of this resuspension is added to 1 mL of Mammalian Ringer's Solution (Electron Microscopy Sciences #11763-10) containing isolated myofibers from the flexor digitorum brevis muscle (FDB) of the mouse foot. The solution containing myofibers and Mitotracker is then pipetted into a 96 well plate (Corning #9017) in increments of 200 µL. This plate is then read at the plate reader for fluorescence with excitation set to 490nm and emission set to 516 nm. Values are then normalized to protein content, assayed in each well after the Mitotracker assay through homogenization and Bradford assay. NMR profiling was performed at the NMR Metabolomics Facility at CCHMC on quadriceps muscle tissues that were snap-frozen within 2 minutes after sacrifice using previously reported protocols (50). Mass-spec profiling of hydrophilic metabolites through untargeted

mass-spec and with $^{13}C$ isotope tracing ex vivo was performed at the Metabolomics Mass-spec Core of Northwestern University using the conditions we detailed previously (30). For $^{13}C$-glucose tracing, we used 25 mU/ml insulin (Cat #RP-10908; Thermo Fisher, Waltham, MA) and 10 mM U-$^{13}C_6$-glucose (Sigma #310808). NMR and mass-spec analyses was performed blinded to treatment groups.

*Mass-spec imaging, i.e. matrix-assisted laser desorption/ionization (MALDI) mass spectrometry.*

Frozen quadriceps muscles were cryosectioned into 12 µm-thick cryosections using a Leica CM1860 cryostat. Cryosections were mounted onto indium tin oxide coated glass slides (Delta Technologies Limited, Loveland, Colorado), then coated with 2′,4′,6′-Trihydroxyacetophenone monohydrate at 10 mg/ml in 50:50 cyclohexane/methanol using a HTX TM Sprayer. 20 passes were performed over each tissue at a spray volume of 50 ml/min and nozzle temperature of 50°C. Once sprayed, samples were individually wrapped in plastic bags and immediately transferred to -80°C. MALDI MS imaging was performed using a Q-Exactive HF mass spectrometer (Thermo Scientific, Bremen, DE) fitted with a MALDI/ESI Injector (Spectroglyph LLC, Kennewick, WA). Laser post-ionization (MALDI-2) was used to enhance analytical sensitivity for triglycerides and cholesteryl esters. Images were acquired at 20 micrometer voxel size, using a pulse energy of ~6 mJ and repetition rate of 30Hz. Q Exactive HF MS Scan parameters were optimized for polar metabolites: polarity – negative, scan range – 350-1500 m/z, resolution – 120,000, automatic gain control – off, maximum inject time 250 ms. ImageInsight™ (Spectroglyph LLC) software was used for initial data visualization and to convert data files into imzML format for visualization and further processing in SciLS™ software (Bruker, Billerica, MA). All metabolite images produced were normalized to the total ion chromatogram.

*Metabolic cages and metabolic treadmill*

$VO_2$ in baseline conditions (ml/h; expressed as aggregate values of l/day) was assessed via indirect calorimetry using the Prometheon Automated Phenotyping System (Sable Systems International, Las Vegas, NV) at the shared Metabolic Cage facility in the CCHMC Vet Services. Data collection started at 24 hours after last prednisone or vehicle injection and lasted for 5 days. Results are expressed as average values (all mice per group, all values per mouse, average of 5 days) over a circadian period, as well as in an ANCOVA analysis (test for difference in

regression lines; performed through CalR(51)) with average values of active phase plotted against body mass values per mouse, as recommended by (52). For $VO_2$ analysis during aerobic exercise, we used an Oxymax Metabolic Treadmill (Columbus Instruments, Columbus, OH), using the stepwise speed increase protocol described previously to separate young vs aged mice based on the slope of the $VO_2$/workload curve and $VO_2$ rates at baseline, submaximal and maximal workloads (40). Treadmill belt was angled 10° uphill to match our regular treadmill conditions and calculate work based on weight. Speed ramp-up was 3-5-8-12-15-17-20-23-25 m/min with stepwise increase every 5min. Mice were assessed at the metabolic treadmill at 24hours after last vehicle or prednisone injection. Metabolic cage and metabolic treadmill assessments were performed blinded to regimens or genotype.

*ChIP-sequencing and RNA-sequencing*

Muscle ChIP was performed using the conditions we previously reported (26). Primary antibody: rabbit polyclonal anti-GR (Abclonal #A2164). Chromatin precipitation: 100µl Dynabeads M-280 (sheep anti-rabbit #11203D; Thermo Scientific, Waltham, MA) per sample. RNA-seq was conducted on RNA extracted from quadriceps muscle. Total RNA was extracted from cryo-pulverized quadriceps muscles with Trizol (#15596026; Thermo Fisher Scientific, Waltham, MA) and re-purified using the Rneasy Mini Kit (Cat #74104; Qiagen, Germantown, MD). Both ChIP-seq and RNA-seq were performed at the CCHMC DNA sequencing Core, generating 20 million or more high quality, 100 base length read pairs per sample. Details regarding library prep and sequencing are available in our GEO datasets (GSE245227, GSE245493). ChIP-seq analysis was conducted using the HOMER software (v4.10, (53); standard commands) after aligning fastq files to the mm10 mouse genome using bowtie2 (54). RNA-seq analysis was performed using kallisto (55) [Version 0.43.1]. PCA was conducted using ClustVis (56). Heatmaps of peak density were imaged with TreeView3 (57). Peak tracks were imaged through WashU epigenome browser. Gene ontology pathway enrichment was conducted using the Gene Ontology analysis tool (58).

*WB, qPCR, OPP, hydroxyproline assays*

Protein analysis was performed on ~50 mg total lysates from whole quadriceps muscles homogenized in general protein buffer, i.e., PBS supplemented with 1 mM $CaCl_2$, 1 mM $MgCl_2$ (#C1016, #M8266, Sigma-Aldrich; St. Louis, MO) and protease and phosphatase inhibitors (#04693232001, #04906837001, Roche, Basel, Switzerland). Blocking and stripping solutions:

StartingBlock and RestorePLUS buffers (#37543, #46430, ThermoFisher Scientific, Waltham, MA). Primary antibodies (all diluted 1:1000 for O/N incubation at +4°C): rabbit anti-PGC1alpha (ABClonal #A12348), rabbit anti-GR (ABClonal #A2164), mouse anti-puromycin (cat# PMY-2A4; DSHB, Iowa City, IA), rabbit anti-GLUD1 (ABClonal #A7631), rabbit anti-GLUL (ABClonal #A21856), rabbit anti-GOT2 (ABClonal #A19245), rabbit anti-GPT2 (ABClonal #A23670), rabbit anti-LIPIN1 (ABClonal #A14111), rabbit anti-Gapdh (ABClonal #AC027), rabbit anti-LC3B (ABClonal #A19665), rabbit anti-Pink1 (ABClonal #A11435), rabbit anti-Mfn2 (ABClonal #A19678), rabbit anti-Fis1 (ABClonal # A19666), total OXPHOS Rodent WB Antibody Cocktail (Abcam #ab110413). Secondary antibodies (diluted 1:5000 for 1-hour incubation at room temperature): HRP-conjugated donkey anti-rabbit or anti-mouse (#sc-2313 and #sc-2314, Santa Cruz Biotech, Dallas, TX). Counterstain for loading control was performed with ponceau (#P7170, Sigma-Aldrich; St. Louis, MO) and/or Gapdh staining. Blots were developed with SuperSignal Pico (cat#34579; Thermo Scientific, Waltham, MA) using the iBrightCL1000 developer system (cat #A32749; Thermo Scientific, Waltham, MA) with automatic exposure settings. WB gels and membranes were run/transferred in parallel and/or stripped for multiple antibody-based staining for densitometry analyses. Protein density was analyzed using the Gel Analysis tool in ImageJ software (59) and expressed as fold changes to control samples.

OPP fluorometry was performed adapting the regular instructions for the Click-iT™ Plus OPP Alexa Fluor™ 488 Protein Synthesis Assay Kit (cat #C10456; Thermo Scientific, Waltham, MA) to live myofibers, isolated from the flexor digitorum brevis (FDB) muscle using previously reported conditions(60). Protein puromycinylation was assessed in gastrocnemius muscle tissue through anti-puromycin WB of whole protein lysates at 30 min post-i.p. puromycin injection (0.040 µmol/body g; #P8833 Sigma-Aldrich; St. Louis, MO).

For RT-qPCR assays, total RNA was reverse-transcribed using 1X qScript Supermix (#95048; QuantaBio, Beverly, MA) and qPCRs were conducted in triplicates using 1X Sybr Green Fast qPCR mix (#RK21200, ABclonal, Woburn, MA) and 100nM primers at a CFX96 qPCR machine (Bio-Rad, Hercules, CA; thermal profile: 95°C, 15 sec; 60°C, 30 sec; 40X; melting curve). Primers were selected among validated primer sets from the MGH Primer Bank; IDs: GPT2-27805389a1; GLUD1-6680027a1; GLUL-31982332a1; GOT2-6754036a1; LIPIN1-27923941a1; and from published primers sets: PGC1a1 and PGc1a4 primers (7); mitochondrial DNA quantification primers (49).

Hydroxyproline content was measured in frozen gastrocnemius muscles as previously described (29). Results were reported as µmol hydroxyproline/100mg tissue. Negative control was an age-matched gastrocnemius from an uninjected WT muscle; positive control was an age-

matched gastrocnemius from an uninjected mdx muscle (JAX #013141)

*Luciferase assays in C2C12 myoblasts*

Luciferase plasmids containing regulatory fragments were obtained cloning genomic sequences in the pGL4.23 backbone (#E8411; Promega), conserving the genomic orientation of the target sequences with regard to transcriptional orientation. Regions were selected as 250bp regions encompassing the canonical GRE (ACAnnnTGT). Control sequences (containing the GRE) and GRE-deleted (missing only the GRE) were generated through custom Gblocks from IDT. Plasmids were then transfected in C2C12 (ATCC #CRL-1772) via Lipofectamine 3000 (#L3000001, Thermo Fisher) together with a Renilla luciferase as internal normalizer. Luciferase signal was then measured as Renilla-normalized Fluc luminescence at 48 hours after either 25µg/ml prednisone or vehicle using the Dual Glo assay (#E2920, Promega). List of tested regions (mm39 coordinates as chromosome, strand, start, end): within the GR peak on the *Pparcg1a* distal TSS (chr5 + 51712172 51712421); within the GR peak on the *Pparcg1a* proximal TSS (chr5 + 51723374 51723623); within the GR peak on the *Lpin1* promoter (chr12 + 16668459 16668708).

*Muscle lipidomics*

Internal standards (Splash Lipidomix, Avanti Polar Lipids, Alabaster, AL, USA) were added to tissue homogenates and lipids were extracted as described previously (61). Lipid identification and quantitation was performed with the methods previously reported (62-64). Lipid species with coefficients of variation greater than 20% between the technical replicates were excluded from further analysis. Analysis for heatmap was based on peak area values normalized to mg tissue.

*AAV preparation and injection*

Approximately 70-80% confluent HEK293T cells (AAVpro® 293T Cell Line; Takara # 632273 AAVpro® 293T Cell Line; Takara # 632273) in DMEM (SH30022.01, Cytiva Life Sciences) supplemented with 2% Bovine Growth Serum (BGS; Cytiva Life Sciences), and 1.0 mM Sodium Pyruvate were triple transfected with pHelper (Cell Biolabs; #340202), pAAV-GOI (Vector Builder; (VB230317-1361ncv; pAAV[Exp]-CMV>mPpargc1a[NM_008904.3]*-V5:WPRE); (VB230317-1364xmj; pAAV[Exp]-CMV>mPpargc1a_isoform4-Myc:WPRE)) and pAAV Rep-Cap (1A-Myo; recloned from published sequence(38), gift from Molkentin lab) plasmids using PEI, Linear, MW250,000 (PolySciences, Inc) in 40-T150mm cell culture plates. Eighteen hours after

transfection, medium is changed to DMEM supplemented with 1% BGS, 1.0 mM Sodium Pyruvate, and 1X MEM Non-essential Amino Acid Solution (Sigma; M7148). Approximately 96 hours post-transfection, the media and cells were collected and processed separately. Cells were lysed using repeated freeze/thaw cycles at a minimum of five times in 1X Gradient Buffer (0.1 M Tris, 0.5 M NaCl, 0.1 M $MgCl_2$). The cell debris were then treated with Benzonase Endonuclease at 0.65 μL per 5 mL (Sigma-Aldrich #1037731010 (100000 Units)) for at least one hour. The homogenates were cleared from debris by centrifugation. AAVs were precipitated from the cell medium with polyethylene glycol (PEG) 8000 The PEG-precipitated AAV was collected by centrifugation, and the AAV pellet was resuspended in 1X GB. Media and cell AAV's were combined and loaded onto an Iodixanol (OptiPrep Density Gradient Medium; Sigma-Aldrich #D1556250) gradient at 15%, 25%, 40% and 60% in 1X Gradient Buffer, and subject to ultracentrifugation. The 40% iodixanol layer, containing the AAV particles, was extracted and a buffer exchange into 2xPBS/10mM MgCl2 was performed using Centrifugal Filters (30000 NMWL (30K), 4.0 mL Sample Volume; Millipore-Sigma #UFC803024, and 100000 NMWL (100K), 15.0 mL Sample Volume; Millipore-Sigma # UFC910024). Primers binding within the AAV-GOI ITR's CMV region (Forward: GTTCCGCGTTACATAACTTACGG; Reverse: CTGCCAAGTGGGCAGTTTACC) were used to measure the virus titer with quantitative polymerase chain reaction (qPCR). Before releasing the viral DNA from the particles, all extra-viral DNA was removed by digestion with DNase I. Then, the viral DNA was released by Proteinase K digestion. For injection, 10^12vg was diluted in 50 μl saline and injected r.o. in anesthetized mice (isoflurane 1.5%) the same day of prednisone injection at week 10 of treatment.

*Statistics*

Statistical analyses were performed using Prism software v9.2.0 (Graphpad, La Jolla, CA). The Pearson-D'Agostino normality test was used to assess data distribution. When comparing data groups for three related variables (age, drug, treatment time; genotype, drug, treatment time), three-way ANOVA was used with pre/post-sample matching and Sidak multi-comparison. When comparing data groups for two related variables, two-way ANOVA was used with Sidak multi-comparison (treatment vs age effect; treatment vs KO effect). Significance scores reported on charts: *, $P<0.05$; **, $P<0.01$; ***, $P<0.001$; ****, $P<0.0001$. When data points < 10, data were presented as single values (dot plots, histograms). Tukey distribution bars or violin plots were used to emphasize data range distribution for > 10 data points per pool. For curves, the s.e.m. values for each plotted point were reported as upper and lower lines.

*Study approval*

Mice were housed in a pathogen-free facility in accordance with the American Veterinary Medical Association (AVMA) and under protocols fully approved by the Institutional Animal Care and Use Committee (IACUC) at Cincinnati Children's Hospital Medical Center (#2022-0020, #2023-0002).

*Data availability*

RNA-seq and ChIP-seq datasets reported here are available on GEO as GSE245227, GSE245493 datasets. Data values for all charts presented can be found in the Supporting Data Values file.

**Author Contributions -** ADP, KMC, KM, HBD, KP, FEAS, HL, CW, HJC, NSB, AJM, BNF: conducting experiments, acquiring data, analyzing data; DPM, BNF: providing reagents, revising the manuscript; MQ: providing reagents, designing research, analyzing data, writing the manuscript.

**Acknowledgements -** NMR profiling was performed thanks to the Cincinnati Children's NMR Metabolomics Facility (RRID: SCR_022636), with critical assistance by Drs. Romick and Watanabe. Mass-spec analyses were performed thanks to the Mass-Spec Metabolomics Core Facility at Robert H. Lurie Comprehensive Cancer Center of Northwestern University, with critical assistance by Dr. Gao. Next-gen sequencing was performed thanks to the Cincinnati Children's DNA Sequencing and Genotyping Facility (RRID: SCR_022630), with critical assistance by David Fletcher, Keely Icardi, Julia Flynn, and Taliesin Lenhart.

**Grant support –** This work was supported by R01AG078174-01, R01HL166356-01, R03DK130908-01A1 (NIH) and RIP, CCRF Endowed Scholarship, HI Translational Funds (CCHMC) grants to MQ; R01HL119225-01A1 (NIH) to BF; R01AG082697 (NIH) to DPM; I01 BX005637, I01 I01BX004671 and IK6 BX006469 (VA) grants to AJM.

## REFERENCES


1. Cruz-Jentoft AJ, Landi F, Topinkova E, and Michel JP. Understanding sarcopenia as a geriatric syndrome. *Curr Opin Clin Nutr Metab Care.* 2010;13(1):1-7.
2. Newman AB, Haggerty CL, Goodpaster B, Harris T, Kritchevsky S, Nevitt M, et al. Strength and muscle quality in a well-functioning cohort of older adults: the Health, Aging and Body Composition Study. *J Am Geriatr Soc.* 2003;51(3):323-30.
3. Short KR, Bigelow ML, Kahl J, Singh R, Coenen-Schimke J, Raghavakaimal S, et al. Decline in skeletal muscle mitochondrial function with aging in humans. *Proc Natl Acad Sci U S A.* 2005;102(15):5618-23.
4. Migliavacca E, Tay SKH, Patel HP, Sonntag T, Civiletto G, McFarlane C, et al. Mitochondrial oxidative capacity and NAD(+) biosynthesis are reduced in human sarcopenia across ethnicities. *Nat Commun.* 2019;10(1):5808.
5. Leveille M, Besse-Patin A, Jouvet N, Gunes A, Sczelecki S, Jeromson S, et al. PGC-1alpha isoforms coordinate to balance hepatic metabolism and apoptosis in inflammatory environments. *Mol Metab.* 2020;34:72-84.
6. Oehler D, Spychala A, Godecke A, Lang A, Gerdes N, Ruas J, et al. Full-length transcriptomic analysis in murine and human heart reveals diversity of PGC-1alpha promoters and isoforms regulated distinctly in myocardial ischemia and obesity. *BMC Biol.* 2022;20(1):169.
7. Ruas JL, White JP, Rao RR, Kleiner S, Brannan KT, Harrison BC, et al. A PGC-1alpha isoform induced by resistance training regulates skeletal muscle hypertrophy. *Cell.* 2012;151(6):1319-31.
8. Guo M, Zhang J, Ma Y, Zhu Z, Zuo H, Yao J, et al. AAV-Mediated nuclear localized PGC1alpha4 delivery in muscle ameliorates sarcopenia and aging-associated metabolic dysfunctions. *Aging Cell.* 2023:e13961.
9. Vina J, Gomez-Cabrera MC, Borras C, Froio T, Sanchis-Gomar F, Martinez-Bello VE, et al. Mitochondrial biogenesis in exercise and in ageing. *Adv Drug Deliv Rev.* 2009;61(14):1369-74.
10. de Smalen LM, Borsch A, Leuchtmann AB, Gill JF, Ritz D, Zavolan M, et al. Impaired age-associated mitochondrial translation is mitigated by exercise and PGC-1alpha. *Proc Natl Acad Sci U S A.* 2023;120(36):e2302360120.
11. Garcia S, Nissanka N, Mareco EA, Rossi S, Peralta S, Diaz F, et al. Overexpression of PGC-1alpha in aging muscle enhances a subset of young-like molecular patterns. *Aging Cell.* 2018;17(2).
12. Sczelecki S, Besse-Patin A, Abboud A, Kleiner S, Laznik-Bogoslavski D, Wrann CD, et al. Loss of Pgc-1alpha expression in aging mouse muscle potentiates glucose intolerance and systemic inflammation. *Am J Physiol Endocrinol Metab.* 2014;306(2):E157-67.
13. Gill JF, Santos G, Schnyder S, and Handschin C. PGC-1alpha affects aging-related changes in muscle and motor function by modulating specific exercise-mediated changes in old mice. *Aging Cell.* 2018;17(1).
14. Yang S, Loro E, Wada S, Kim B, Tseng WJ, Li K, et al. Functional effects of muscle PGC-1alpha in aged animals. *Skelet Muscle.* 2020;10(1):14.
15. Schweitzer GG, Collier SL, Chen Z, McCommis KS, Pittman SK, Yoshino J, et al. Loss of lipin 1-mediated phosphatidic acid phosphohydrolase activity in muscle leads to skeletal myopathy in mice. *FASEB J.* 2019;33(1):652-67.
16. Ren H, Federico L, Huang H, Sunkara M, Drennan T, Frohman MA, et al. A phosphatidic acid binding/nuclear localization motif determines lipin1 function in lipid metabolism and adipogenesis. *Mol Biol Cell.* 2010;21(18):3171-81.
17. Han GS, Wu WI, and Carman GM. The Saccharomyces cerevisiae Lipin homolog is a Mg2+-dependent phosphatidate phosphatase enzyme. *J Biol Chem.* 2006;281(14):9210-8.
18. Finck BN, Gropler MC, Chen Z, Leone TC, Croce MA, Harris TE, et al. Lipin 1 is an inducible amplifier of the hepatic PGC-1alpha/PPARalpha regulatory pathway. *Cell Metab.* 2006;4(3):199-210.
19. Jama A, Alshudukhi AA, Burke S, Dong L, Kamau JK, Voss AA, et al. Lipin1 plays complementary roles in myofibre stability and regeneration in dystrophic muscles. *J Physiol.* 2023;601(5):961-78.
20. Zhang P, Verity MA, and Reue K. Lipin-1 regulates autophagy clearance and intersects with statin drug effects in skeletal muscle. *Cell Metab.* 2014;20(2):267-79.
21. Alshudukhi AA, Zhu J, Huang D, Jama A, Smith JD, Wang QJ, et al. Lipin-1 regulates Bnip3-mediated mitophagy in glycolytic muscle. *FASEB J.* 2018;32(12):6796-807.
22. Schacke H, Docke WD, and Asadullah K. Mechanisms involved in the side effects of glucocorticoids. *Pharmacology & therapeutics.* 2002;96(1):23-43.

23. Quattrocelli M, Wintzinger M, Miz K, Panta M, Prabakaran AD, Barish GD, et al. Intermittent prednisone treatment in mice promotes exercise tolerance in obesity through adiponectin. *J Exp Med.* 2022;219(5).
24. Zelikovich AS, Joslin BC, Casey P, McNally EM, and Ajroud-Driss S. An Open Label Exploratory Clinical Trial Evaluating Safety and Tolerability of Once-Weekly Prednisone in Becker and Limb-Girdle Muscular Dystrophy. *J Neuromuscul Dis.* 2022;9(2):275-87.
25. Dao T, Green AE, Kim YA, Bae SJ, Ha KT, Gariani K, et al. Sarcopenia and Muscle Aging: A Brief Overview. *Endocrinol Metab (Seoul).* 2020;35(4):716-32.
26. Quattrocelli M, Wintzinger M, Miz K, Levine DC, Peek CB, Bass J, et al. Muscle mitochondrial remodeling by intermittent glucocorticoid drugs requires an intact circadian clock and muscle PGC1alpha. *Sci Adv.* 2022;8(7):eabm1189.
27. Sakamuri S, Sperling JA, Sure VN, Dholakia MH, Peterson NR, Rutkai I, et al. Measurement of respiratory function in isolated cardiac mitochondria using Seahorse XFe24 Analyzer: applications for aging research. *Geroscience.* 2018;40(3):347-56.
28. Olesen AT, Malchow-Moller L, Bendixen RD, Kjaer M, Svensson RB, Andersen JL, et al. Age-related myofiber atrophy in old mice is reversed by ten weeks voluntary high-resistance wheel running. *Exp Gerontol.* 2021;143:111150.
29. Quattrocelli M, Salamone IM, Page PG, Warner JL, Demonbreun AR, and McNally EM. Intermittent Glucocorticoid Dosing Improves Muscle Repair and Function in Mice with Limb-Girdle Muscular Dystrophy. *Am J Pathol.* 2017;187(11):2520-35.
30. Quattrocelli M, Zelikovich AS, Jiang Z, Peek CB, Demonbreun AR, Kuntz NL, et al. Pulsed glucocorticoids enhance dystrophic muscle performance through epigenetic-metabolic reprogramming. *JCI Insight.* 2019;4(24).
31. Lin J, Wu PH, Tarr PT, Lindenberg KS, St-Pierre J, Zhang CY, et al. Defects in adaptive energy metabolism with CNS-linked hyperactivity in PGC-1alpha null mice. *Cell.* 2004;119(1):121-35.
32. McCarthy JJ, Srikuea R, Kirby TJ, Peterson CA, and Esser KA. Inducible Cre transgenic mouse strain for skeletal muscle-specific gene targeting. *Skelet Muscle.* 2012;2(1):8.
33. Li Y, Ji X, Chang L, Tang J, Hua MM, Liu J, et al. Click-iT ((R)) Plus OPP Alexa Fluor ((R)) Protein Synthesis Assay in Embryonic Cells. *Bio Protoc.* 2022;12(11):e4441.
34. Fujita S, and Volpi E. Amino acids and muscle loss with aging. *J Nutr.* 2006;136(1 Suppl):277S-80S.
35. Kamei Y, Hatazawa Y, Uchitomi R, Yoshimura R, and Miura S. Regulation of Skeletal Muscle Function by Amino Acids. *Nutrients.* 2020;12(1).
36. Summermatter S, Santos G, Perez-Schindler J, and Handschin C. Skeletal muscle PGC-1alpha controls whole-body lactate homeostasis through estrogen-related receptor alpha-dependent activation of LDH B and repression of LDH A. *Proc Natl Acad Sci U S A.* 2013;110(21):8738-43.
37. Hatazawa Y, Qian K, Gong DW, and Kamei Y. PGC-1alpha regulates alanine metabolism in muscle cells. *PloS one.* 2018;13(1):e0190904.
38. Tabebordbar M, Lagerborg KA, Stanton A, King EM, Ye S, Tellez L, et al. Directed evolution of a family of AAV capsid variants enabling potent muscle-directed gene delivery across species. *Cell.* 2021;184(19):4919-38 e22.
39. Agudelo LZ, Ferreira DMS, Dadvar S, Cervenka I, Ketscher L, Izadi M, et al. Skeletal muscle PGC-1alpha1 reroutes kynurenine metabolism to increase energy efficiency and fatigue-resistance. *Nat Commun.* 2019;10(1):2767.
40. Schefer V, and Talan MI. Oxygen consumption in adult and AGED C57BL/6J mice during acute treadmill exercise of different intensity. *Exp Gerontol.* 1996;31(3):387-92.
41. Salamone IM, Quattrocelli M, Barefield DY, Page PG, Tahtah I, Hadhazy M, et al. Intermittent glucocorticoid treatment enhances skeletal muscle performance through sexually dimorphic mechanisms. *J Clin Invest.* 2022;132(6).
42. Paez HG, Pitzer CR, and Alway SE. Age-Related Dysfunction in Proteostasis and Cellular Quality Control in the Development of Sarcopenia. *Cells.* 2023;12(2).
43. Chambers KT, Cooper MA, Swearingen AR, Brookheart RT, Schweitzer GG, Weinheimer CJ, et al. Myocardial Lipin 1 knockout in mice approximates cardiac effects of human LPIN1 mutations. *JCI Insight.* 2021;6(9).
44. Hosios AM, Hecht VC, Danai LV, Johnson MO, Rathmell JC, Steinhauser ML, et al. Amino Acids Rather than Glucose Account for the Majority of Cell Mass in Proliferating Mammalian Cells. *Dev Cell.* 2016;36(5):540-9.

45. Martinez-Reyes I, and Chandel NS. Mitochondrial TCA cycle metabolites control physiology and disease. *Nat Commun.* 2020;11(1):102.
46. Markofski MM, Jennings K, Timmerman KL, Dickinson JM, Fry CS, Borack MS, et al. Effect of Aerobic Exercise Training and Essential Amino Acid Supplementation for 24 Weeks on Physical Function, Body Composition, and Muscle Metabolism in Healthy, Independent Older Adults: A Randomized Clinical Trial. *The journals of gerontology Series A, Biological sciences and medical sciences.* 2019;74(10):1598-604.
47. Lopez-Otin C, Blasco MA, Partridge L, Serrano M, and Kroemer G. The hallmarks of aging. *Cell.* 2013;153(6):1194-217.
48. Durumutla HB, Villa C, Panta M, Wintzinger M, Pragasam ADP, Miz K, et al. Comprehensive Analyses of Muscle Function, Lean and Muscle Mass, and Myofiber Typing in Mice. *Bio Protoc.* 2023;13(4):e4617.
49. Quiros PM, Goyal A, Jha P, and Auwerx J. Analysis of mtDNA/nDNA Ratio in Mice. *Curr Protoc Mouse Biol.* 2017;7(1):47-54.
50. Kwong JQ, Huo J, Bround MJ, Boyer JG, Schwanekamp JA, Ghazal N, et al. The mitochondrial calcium uniporter underlies metabolic fuel preference in skeletal muscle. *JCI Insight.* 2018;3(22).
51. Mina AI, LeClair RA, LeClair KB, Cohen DE, Lantier L, and Banks AS. CalR: A Web-Based Analysis Tool for Indirect Calorimetry Experiments. *Cell Metab.* 2018;28(4):656-66 e1.
52. Tschop MH, Speakman JR, Arch JR, Auwerx J, Bruning JC, Chan L, et al. A guide to analysis of mouse energy metabolism. *Nat Methods.* 2011;9(1):57-63.
53. Heinz S, Benner C, Spann N, Bertolino E, Lin YC, Laslo P, et al. Simple combinations of lineage-determining transcription factors prime cis-regulatory elements required for macrophage and B cell identities. *Mol Cell.* 2010;38(4):576-89.
54. Langmead B, and Salzberg SL. Fast gapped-read alignment with Bowtie 2. *Nat Methods.* 2012;9(4):357-9.
55. Bray NL, Pimentel H, Melsted P, and Pachter L. Near-optimal probabilistic RNA-seq quantification. *Nat Biotechnol.* 2016;34(5):525-7.
56. Metsalu T, and Vilo J. ClustVis: a web tool for visualizing clustering of multivariate data using Principal Component Analysis and heatmap. *Nucleic Acids Res.* 2015;43(W1):W566-70.
57. Saldanha AJ. Java Treeview--extensible visualization of microarray data. *Bioinformatics.* 2004;20(17):3246-8.
58. Ashburner M, Ball CA, Blake JA, Botstein D, Butler H, Cherry JM, et al. Gene ontology: tool for the unification of biology. The Gene Ontology Consortium. *Nat Genet.* 2000;25(1):25-9.
59. Schneider CA, Rasband WS, and Eliceiri KW. NIH Image to ImageJ: 25 years of image analysis. *Nat Methods.* 2012;9(7):671-5.
60. Demonbreun AR, and McNally EM. DNA Electroporation, Isolation and Imaging of Myofibers. *J Vis Exp.* 2015(106):e53551.
61. Deng P, Hoffman JB, Petriello MC, Wang CY, Li XS, Kraemer MP, et al. Dietary inulin decreases circulating ceramides by suppressing neutral sphingomyelinase expression and activity in mice. *J Lipid Res.* 2020;61(1):45-53.
62. Kipp ZA, Martinez GJ, Bates EA, Maharramov AB, Flight RM, Moseley HNB, et al. Bilirubin Nanoparticle Treatment in Obese Mice Inhibits Hepatic Ceramide Production and Remodels Liver Fat Content. *Metabolites.* 2023;13(2).
63. Khan MJ, Codreanu SG, Goyal S, Wages PA, Gorti SKK, Pearson MJ, et al. Evaluating a targeted multiple reaction monitoring approach to global untargeted lipidomic analyses of human plasma. *Rapid Commun Mass Spectrom.* 2020;34(22):e8911.
64. Zhang Z, Singh M, Kindt A, Wegrzyn AB, Pearson MJ, Ali A, et al. Development of a targeted hydrophilic interaction liquid chromatography-tandem mass spectrometry based lipidomics platform applied to a coronavirus disease severity study. *J Chromatogr A.* 2023;1708:464342.

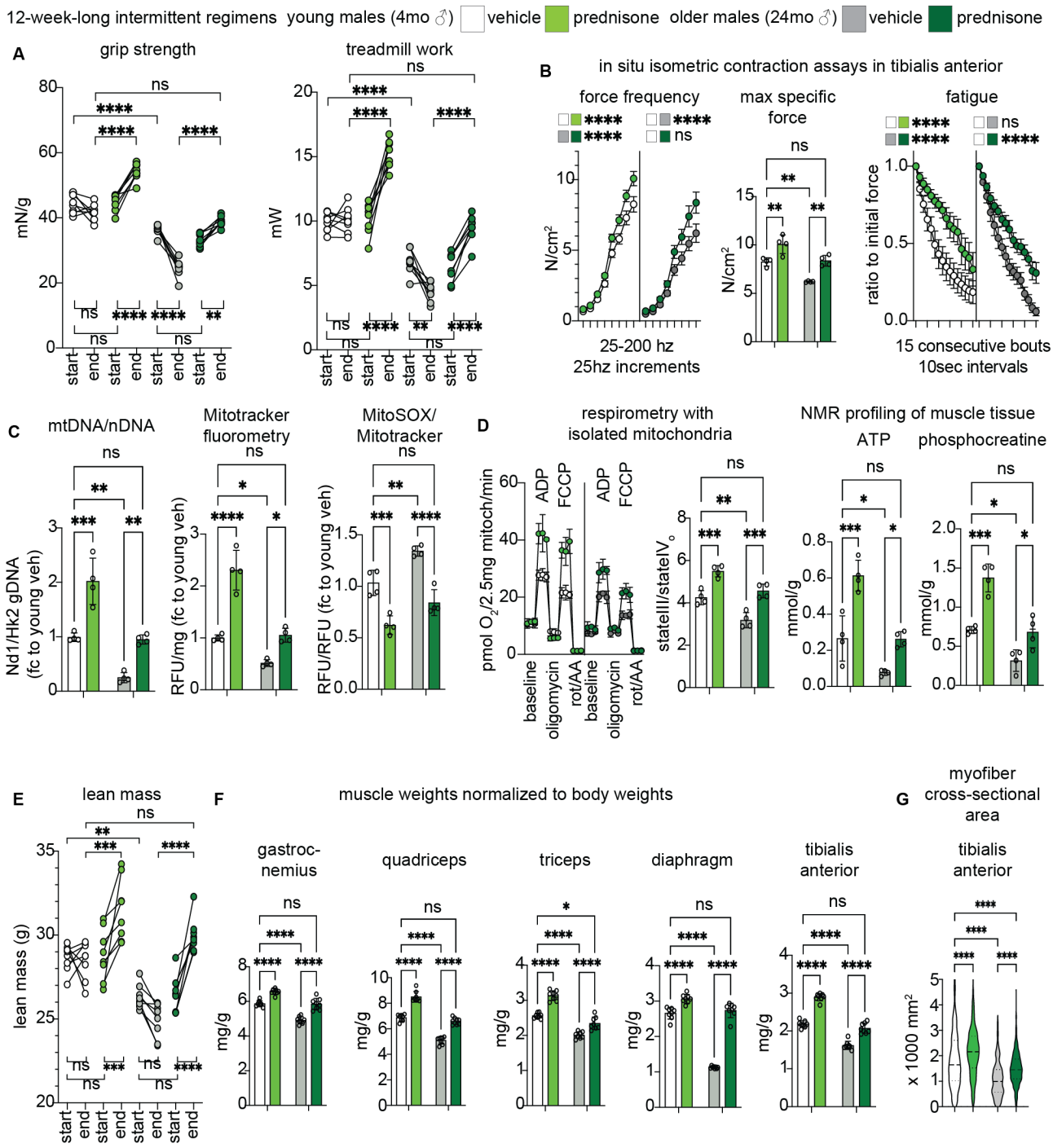


**Figure 1. Intermittent once-weekly prednisone regimen rejuvenates mitochondrial and mass properties of the aging muscle. (A)** Treatment improved strength and treadmill performance in background-matched male mice at young adult (4mo) and older adult (24mo) ages, improving the parameters of treated aged mice to levels comparable to the control (vehicle) young adult mice at endpoint. **(B)** Treatment rescued specific force in older mice to control young levels, while increasing resistance to repetitive tetanus fatigue to comparable extent at both ages. **(C-D)** Treatment improved mitochondrial abundance (mtDNA/nDNA, Mitotracker) and decreased superoxide levels (MitoSOX) in aged muscle to young control-like levels. Analogous trends were observed with mitochondrial respiration levels and NMR-quantitated levels of ATP and phosphocreatine in quadriceps muscles. **(E-G)** In treated older mice, total lean mass increased to young control-like levels. This correlated with rescue of muscle weight/body weight ratios in older mice in locomotory (gastrocnemius, quadriceps, triceps) and respiratory (diaphragm) muscles. Tibialis anterior muscle analyses showed coupling of myofiber CSA trends with the changes in muscle mass. N=4-8/group; histograms and curves report mean±s.e.m., pre-post plots report each subject trend, violin plots indicate mean and 25-75 percentiles; (start-end) pre/post-paired 3w ANOVA + Sidak; (endpoint) 2w ANOVA + Sidak: *, P<0.05; **, P<0.01; ***, P<0.001; ****, P<0.0001.

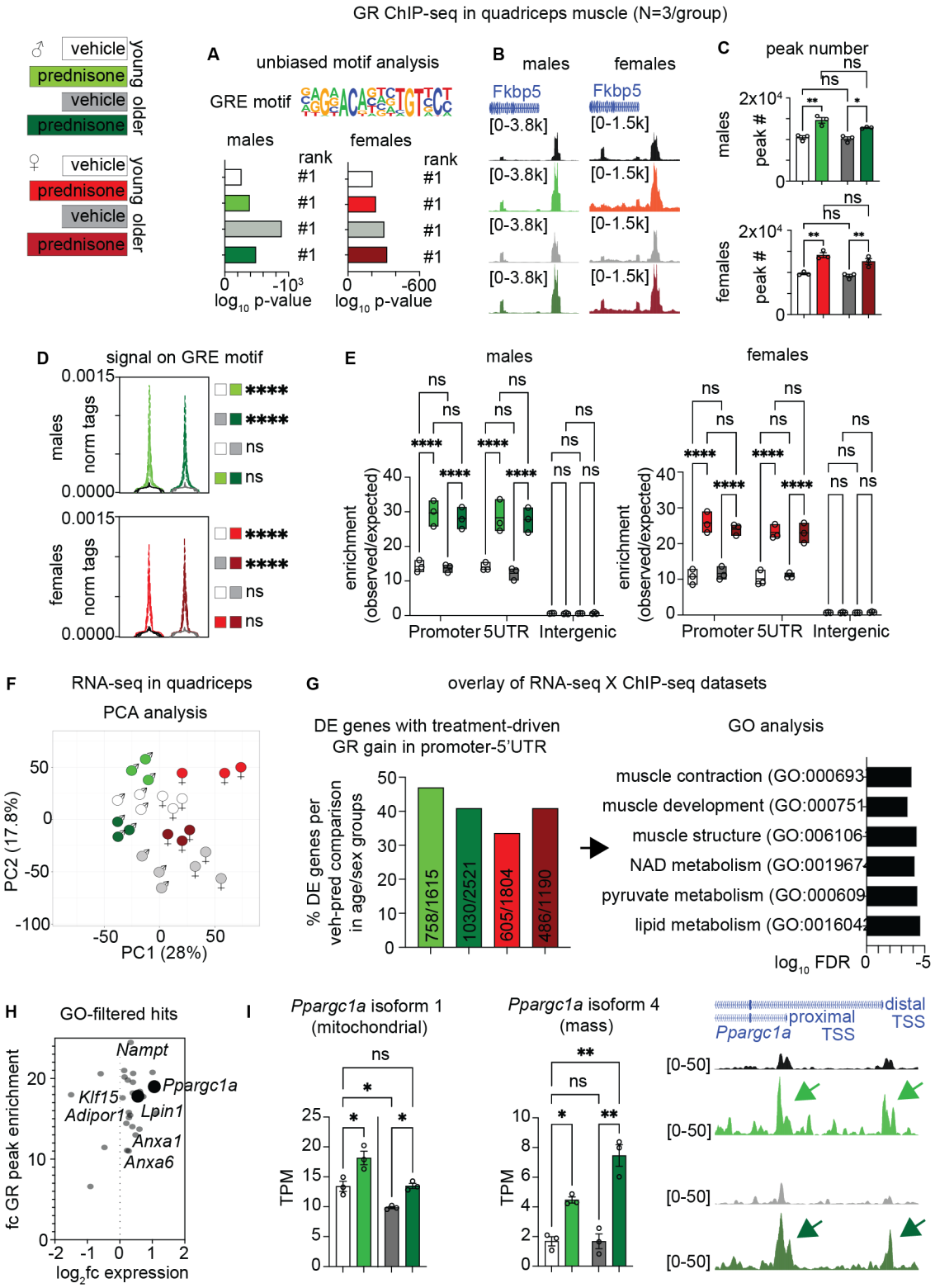


**Figure 2. Epigenetic and transcriptional profiling reveals a treatment-induced muscle GR cistrome that is maintained through aging. (A-B)** Motif analysis and robust promoter peaks in the canonical target *Fkbp5* confirm GR ChIP-seq datasets. **(C-E)** Treatment increased GR peak number and genome-wide, GRE-bound GR signal to comparable extents in both age (young, older) groups in both males and females. In all experimental groups, treatment increased GR signal in promoters and 5'UTR regions. **(F)** PCA analysis of RNA-seq datasets showed age- and treatment-related trends across sexes. **(G-H)** GO analysis revealed enrichment for muscle metabolic factors, particularly *Ppargc1a* (encoding PGC1alpha) and *Lpin1* (encoding the PGC1alpha co-factor Lipin1). **(I)** Expression of both isoforms 1 and 4 of *Ppargc1a* was rescued to young-like levels in treated older muscle, correlating with increased GR binding on canonical and alternative start sites (arrows). N=3/group; histograms report mean±s.e.m.; 2w ANOVA + Sidak: *, P<0.05; **, P<0.01; ***, P<0.001; ****, P<0.0001.

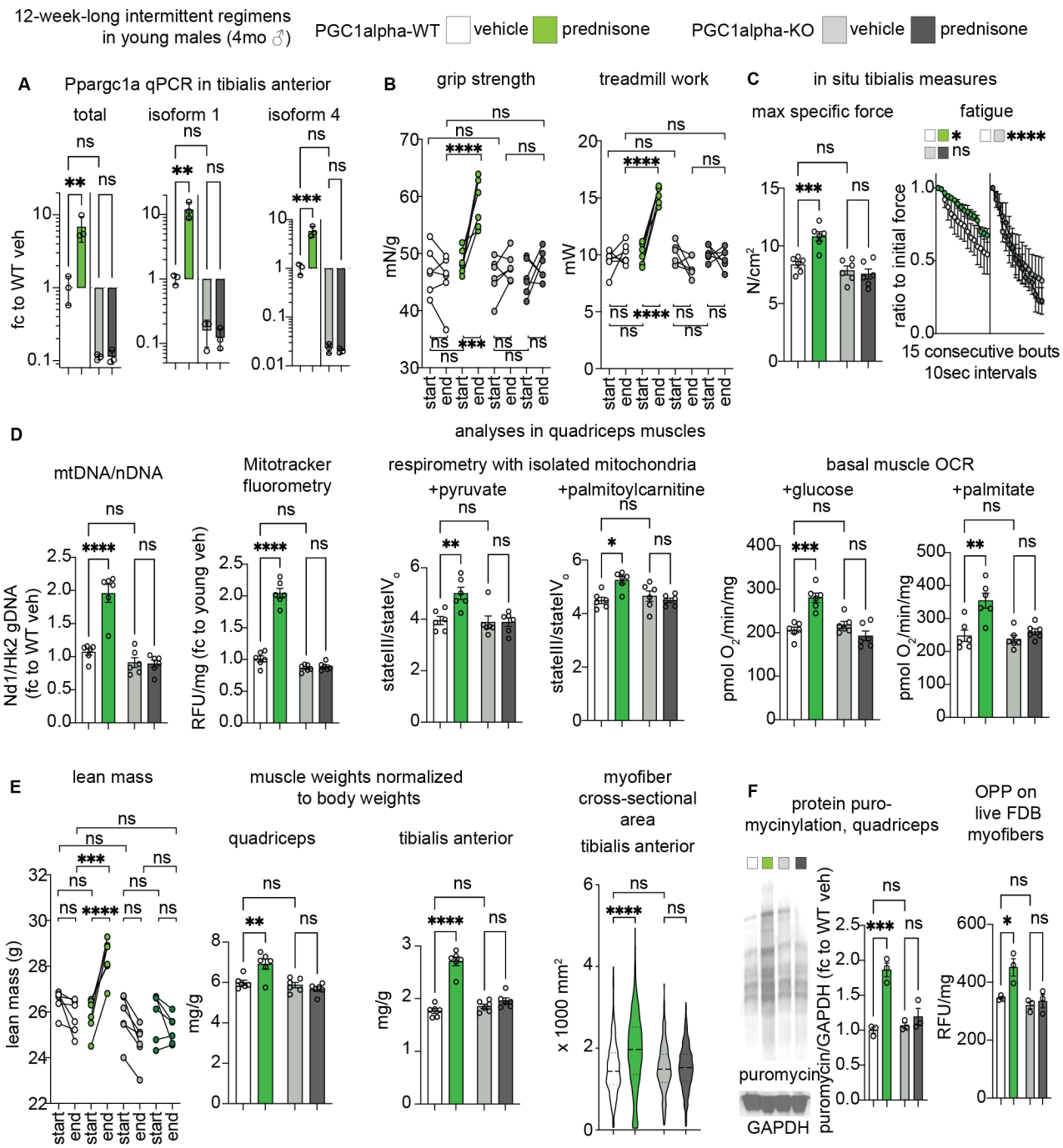


**Figure 3. Myocyte-specific inducible PGC1alpha ablation blocks treatment effects on both mitochondrial function and muscle mass. (A)** Recombination of the floxed allele reduced expression of both PGC1alpha isoforms in muscle. **(B-C)** In young adult mice, myocyte-specific inducible PGC1alpha ablation blocked the effects of 12-week-long intermittent prednisone treatment on strength, treadmill, force, and fatigue. **(D)** PGC1alpha ablation blocked or blunted treatment effects on mitochondrial abundance and on mitochondrial RCR and basal OCR in muscle tissue regardless of fuel. **(E)** PGC1alpha ablation blocked or blunted treatment effects on lean mass, muscle mass, myofiber CSA. **(F)** Treatment increased protein translation in muscle dependent on myocyte PGC1alpha. N=3-6/group; histograms and curves report mean±s.e.m., pre-post plots report each subject trend, violin plots indicate mean and 25-75 percentiles; (start-end) pre/post-paired 3w ANOVA + Sidak; (endpoint) 2w ANOVA + Sidak: *, P<0.05; **, P<0.01; ***, P<0.001; ****, P<0.0001.

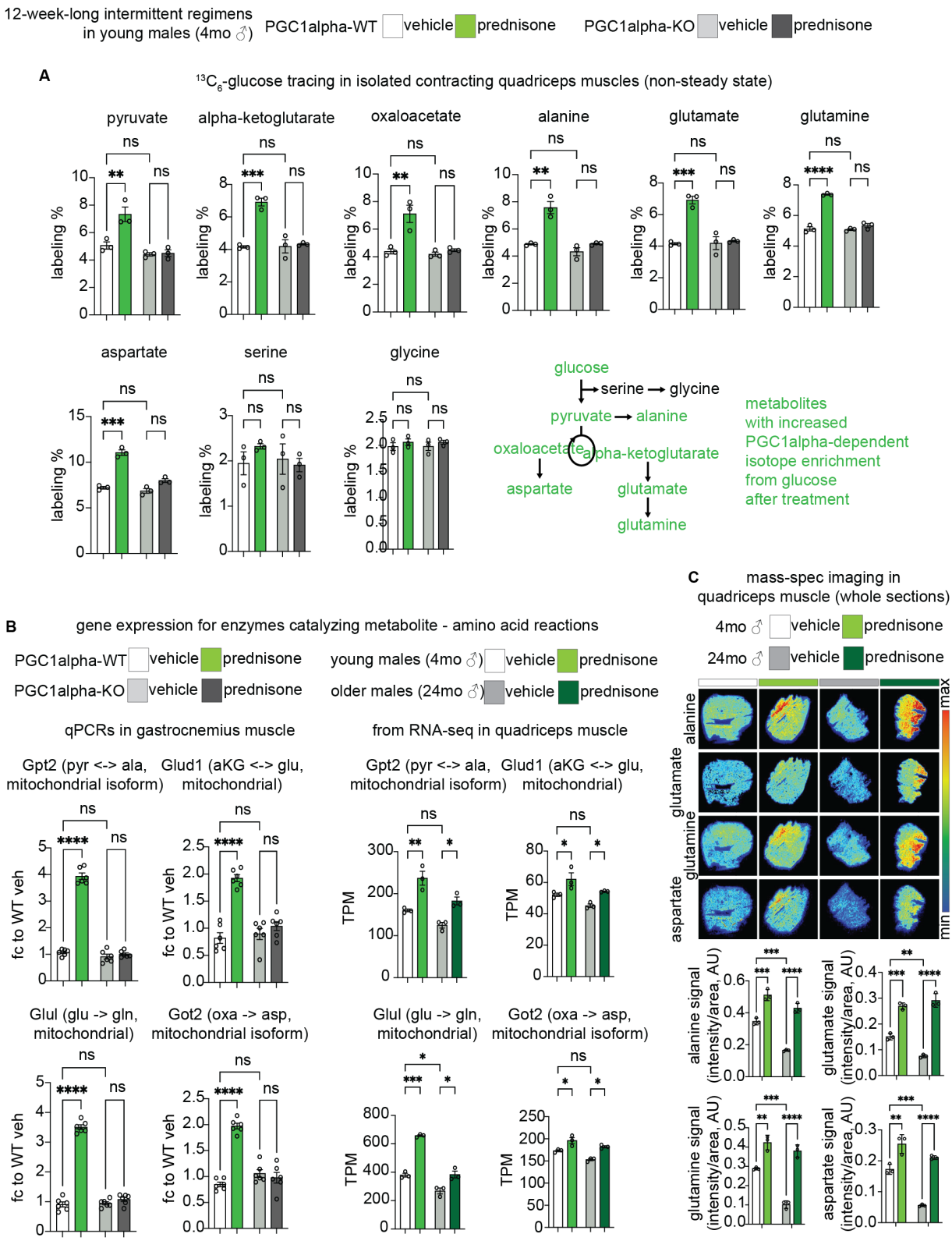


**Figure 4. Treatment increases carbon shuttling between glucose and amino acids in muscle dependent on myocyte-specific PGC1alpha. (A)** In isolated contracting muscle exposed to $^{13}C_6$-glucose, treatment increased carbon shuttling to alanine, glutamate, glutamine, aspartate, but not to serine, glycine. **(B)** Myocyte-specific PGC1alpha was required for treatment-driven upregulation of mitochondrial enzymes and/or enzyme isoforms mediating the underlying reactions between glucose derivatives and amino acids. The treatment effect on expression of those genes was also confirmed in young and older muscles per RNA-seq. **(C)** Mass-spec imaging showed increased levels of target amino acids in treated young and aged muscles after a glucose+insulin challenge. N=3-6/group; histograms report mean±s.e.m.;2w ANOVA + Sidak: *, P<0.05; **, P<0.01; ***, P<0.001; ****, P<0.0001.

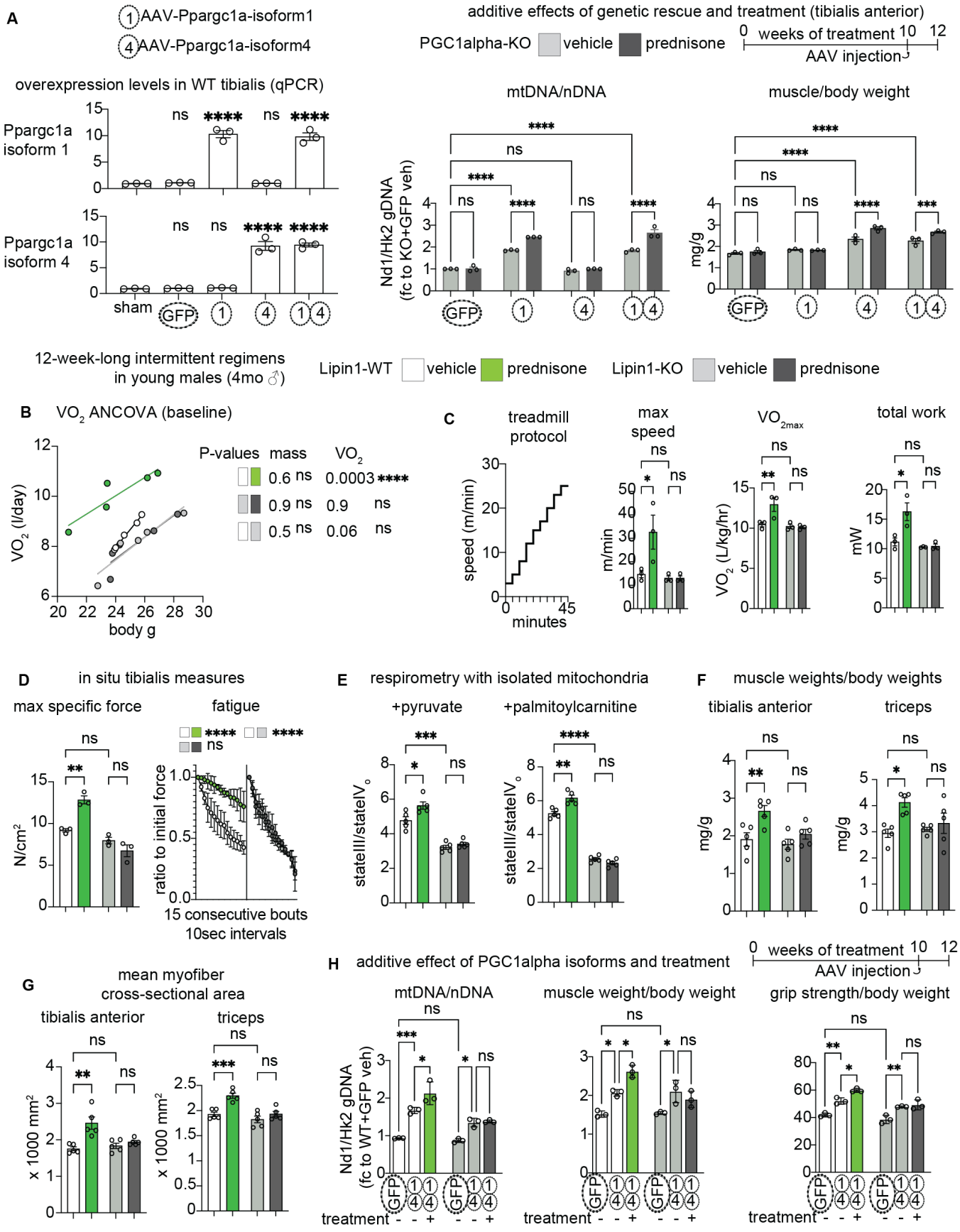
A
1 AAV-Ppargc1a-isoform1
4 AAV-Ppargc1a-isoform4
overexpression levels in WT tibialis (qPCR)
Ppargc1a isoform 1
Ppargc1a isoform 4
sham
GFP
additive effects of genetic rescue and treatment (tibialis anterior)
PGC1alpha-KO
vehicle
prednisone
0 weeks of treatment 10 12
AAV injection
mtDNA/nDNA
Nd1/Hk2 gDNA (fc to KO+GFP veh)
muscle/body weight
mg/g
12-week-long intermittent regimens in young males (4mo ♂)
Lipin1-WT
vehicle
prednisone
Lipin1-KO
vehicle
prednisone
B
VO2 ANCOVA (baseline)
VO2 (l/day)
body g
P-values mass VO2
0.6 ns 0.0003 ****
0.9 ns 0.9 ns
0.5 ns 0.06 ns
C
treadmill protocol
speed (m/min)
minutes
max speed
m/min
VO2max
VO2 (L/kg/hr)
total work
mW
D
in situ tibialis measures
max specific force
N/cm2
fatigue
ratio to initial force
15 consecutive bouts
10sec intervals
E
respirometry with isolated mitochondria
+pyruvate
+palmitoylcarnitine
stateIII/stateIVo
F
muscle weights/body weights
tibialis anterior
triceps
mg/g
G
mean myofiber cross-sectional area
tibialis anterior
triceps
x 1000 mm2
H
additive effect of PGC1alpha isoforms and treatment
0 weeks of treatment 10 12
AAV injection
mtDNA/nDNA
Nd1/Hk2 gDNA (fc to WT+GFP veh)
muscle weight/body weight
grip strength/body weight
treatment

**Figure 5. Myocyte-specific Lipin1 controls energy-mass balance in muscle. (A)** MyoAAV-mediated overexpression in WT muscle at 2 weeks post r.o. injection of 10^12vg/mouse (left). Combination of AAV and treatment in PGC1alpha-KO mice revealed an additive effect of treatment on genetic rescues of mitochondrial abundance by Pgc1alpha isoform 1 and muscle mass by Pgc1alpha isoform 4 (right) in tibialis anterior muscles. Together with our RNA-seq/ChIP-seq screening, the additive effect warranted investigation of Lipin1 as treatment-driven co-factor to coax PGC1alpha regulation with energy-mass balance. **(B)** ANCOVA analysis for VO2 in metabolic cages without specific exercise triggers showed increased $VO_2$ independent from body mass in control mice (Lipin1-WT), but not after Lipin1 ablation (Lipin1-KO). **(C)** In the metabolic treadmill, treatment increased $VO_{2max}$, as well as speed and work at exhaustion dependent on myocyte-specific Lipin1. **(D-E)** Lipin1 was critical for treatment-driven effects on muscle force and fatiguability, and mitochondrial respiration. **(F-G)** Analogously to its co-factor PGC1alpha manipulation, Lipin1 ablation blunted or blocked treatment effects on muscle mass in two different locomotory muscles (tibialis, hindlimbs; triceps, forelimbs). **(H)** Lipin1-KO blocked the additive effect of treatment on top of the PGC1alpha isoform 1+4 overexpression effect on mitochondrial abundance and muscle mass of tibialis anterior, and grip strength. N=3-5/group; histograms and curves report mean±s.e.m.; 2w ANOVA + Sidak: *, P<0.05; **, P<0.01; ***, P<0.001; ****, P<0.0001.